DOI: 10.1002/chem.201000620

Characterization, Direct Electrochemistry, and Amperometric Biosensing of Graphene by Noncovalent Functionalization with Picket-Fence Porphyrin

Wenwen Tu, Jianping Lei,* Siyuan Zhang, and Huangxian Ju*[a]

Abstract: Reduced graphene oxide (RGO) was prepared and functionalized with picket-fence porphyrin, 5,10,15,20-tetrakis [αααα-2-trismethylammoniomethylphenyl] porphyrin iron(III) pentachloride (FeTMAPP), through π–π interactions. The resulting nanocomposite was characterized by atomic force microscopy (AFM); transmission electron microscopy (TEM); contact angle measurements; and fluorescence, Raman, and UV/Vis absorption spectroscopy. On account of the introduction of positively charged FeTMAPP, the functionalized RGO showed good dispersion in aqueous solution. The RGO could greatly accelerate the electron transfer of FeTMAPP to produce a well-defined redox couple of Fe^{III}/Fe^{II} at −0.291 and −0.314 V. Due to the synergic effect between RGO and the porphyrin, the nanocomposite showed excellent electrocatalytic activity toward the reduction of chlorite, thus leading to highly sensitive amperometric biosensing at low applied potential. The biosensor for chlorite showed a linear range from 5.0×10^{-8} to 1.2×10^{-4} mol L^{-1} with a detection limit of 2.4×10^{-8} mol L^{-1} at a signal-to-noise ratio of 3. The picket-fence porphyrin could serve as an efficient species to functionalize graphene for electronic and optical applications.

Keywords: electrochemistry · graphene · nanostructures · pi interactions · porphyrinoids

Introduction

Graphene, a single-layered two-dimensional (2D) sheet, has attracted enthusiastic interest in many areas of nanoscience and nanotechnology due to its fascinating physical properties such as great mechanical strength, fast electron transfer, universal optical absorption, and high specific surface area.[1–12] Usually, graphene oxide (GO) can be easily deposited on different substrates to produce continuous films for the construction of transparent conductors,[13] photovoltaic devices,[14–16] and biosensors,[17–19] since GO sheets decorated with oxygen functional groups can be readily exfoliated to form a stable aqueous dispersion.[15,20–22] However, the numerous oxygen functional groups of GO render it too electrically insulating for a conductance-based device.[23] Thus, reduced graphene oxide (RGO), achieved by means of chemical reduction using hydrazine hydrate to remove oxygen and recover the aromatic double-bonded carbon atoms,[22,23] is another promising candidate for the construction of electronic and optical devices. However, due to the lack of solubility and active sites on the sheet, it is of the utmost importance to functionalize RGO for further applications.

The functionalization of RGO with various molecules to enhance their solubility and self-assembly properties can be performed by covalent[24–28] or noncovalent methods.[29–33] The latter is particularly promising, since the graphene functionalized through noncovalent modification can retain its electronic structure. For example, the graphene sheets prepared by the reduction of GO have been noncovalently functionalized with negatively charged 1-pyrenebutyrate through π–π interactions, thereby resulting in a conductivity seven orders of magnitude larger than the GO precursor.[30] Based on the supramolecular assembly of free-base 5,10,15,20-tetrakis(*N*-methylpyridinum-4-yl)porphyrin tetra(*p*-toluenesulfonate) on RGO, an optical probe has been constructed for sensing Cd^{2+} ions.[31]

Compared with simple and free-base arylporphyrin, picket-fence porphyrin, a kind of metalloporphyrin, has a macrocyclic porphin ring with four columnlike phenyl substitutes and can simulate the active centers of some proteins and enzymes, which leads to better catalytic activity toward biomolecules.[34–37] In particular, the metalloporphyrin has been well used as electron media and exhibits good electro-

[a] W. Tu, Dr. J. Lei, S. Zhang, Prof. H. Ju
MOE Key Laboratory of Analytical Chemistry for Life Science
School of Chemistry and Chemical Engineering
Nanjing University, Nanjing 210093 (P.R. China)
Fax: (+86) 25-8359-3593
E-mail: jpl@nju.edu.cn
hxju@nju.edu.cn

catalysis toward the reduction or oxidation of many small molecules related to life process.[38–41] This work used water-soluble 5,10,15,20-tetrakis [αααα-2-trismethylammoniomethylphenyl]porphyrin iron(III) pentachloride (FeTMAPP), a kind of picket-fence porphyrin with one planar side and another positively charged side, to functionalize RGO by means of π–π noncovalent interactions (Scheme 1). The obtained porphyrin/RGO nanocomposite showed good dispersion. The fast direct electron transfer between FeTMAPP and the electrode could be obtained due to the presence of RGO. The synergic effect between RGO and porphyrin led to highly efficient electrocatalytic activity for the reduction of chlorite.

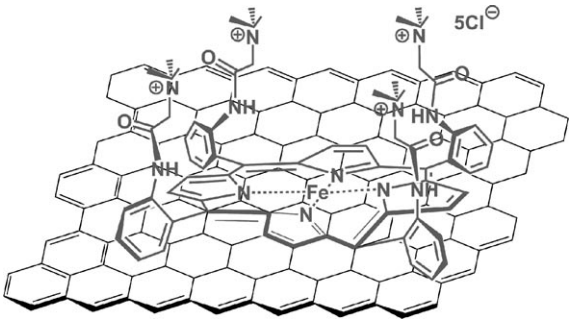

Scheme 1. Schematic representation of the noncovalent assembly of FeTMAPP on RGO.

Chlorite, as a by-product of drinking water disinfection, may cause hemolytic anemia at low levels of exposure, whereas higher levels of exposure can result in an increase of methemoblobin. Thus, the World Health Organization has published the guideline value of 2.6×10^{-7} mol L^{-1} for chlorite monitoring.[42] Several methods such as capillary electrophoresis,[43] the ion chromatographic method,[44] and potentiometric technique[45] have been developed for chlorite detection. Although these methods have adequate sensitivity, they often suffer from time-consuming derivatization and extraction processes, as well as professional operation. It is especially difficult to use these methods for in situ or online monitoring. Based on the highly efficient catalysis of porphyrin-functionalized RGO, this work developed a sensitive amperometric biosensor for chlorite. This biosensor showed promising application in the monitoring of chlorite with low cost, convenient operation, high sensitivity, and a wide concentration range. The noncovalent functionalization of RGO with porphyrin provides a convenient way to construct a novel biosensing platform, and extends the application of graphene in bioanalysis.

Results and Discussion

Atomic force and transmission electron microscopic images of FeTMAPP/RGO: The atomic force microscopic (AFM) image was used to characterize the FeTMAPP/RGO nanocomposite sheet. As shown in Figure 1A, the average thickness of RGO aggregations was measured to be about 6.5 nm due to the poor dispersion of RGO sheets in water. Considering that the thickness of a clean graphene sheet is 0.7 nm,[20] it was about 9 layers of RGO sheet. However, when RGO was functionalized with FeTMAPP, the average thickness of a FeTMAPP/RGO sheet was determined to be about 1.2 nm (Figure 1B) due to the introduction of positively charged FeTMAPP on RGO. By considering that the thickness of one porphyrin molecule is about 0.5 nm,[46] it could be concluded that a monolayer of FeTMAPP molecules was assembled on a monolayer of RGO. The transmission electron microscopy (TEM) image revealed few-layer flexible wrinkled sheets of the RGO situated on the top of the copper grid (Figure 1C), illustrating the flakelike shape of RGO.[11,47] The single-sheet nature shown in Figure 1D identified the better dispersion of FeTMAPP/RGO in water. Furthermore, the introduction of positively charged FeTMAPP on RGO led to a stable black suspension of FeTMAPP/RGO, whereas the suspension of RGO was unstable (Figure 1E), which indicates a good dispersion of the nanocomposite. The deeper color of FeTMAPP/RGO than both FeTMAPP and RGO dispersions also suggested the formation of a homogeneous nanocomposite. At the concentration of 0.1 mg mL^{-1}, the dispersion of FeTMAPP/RGO was very stable, even for a storage period of several weeks.

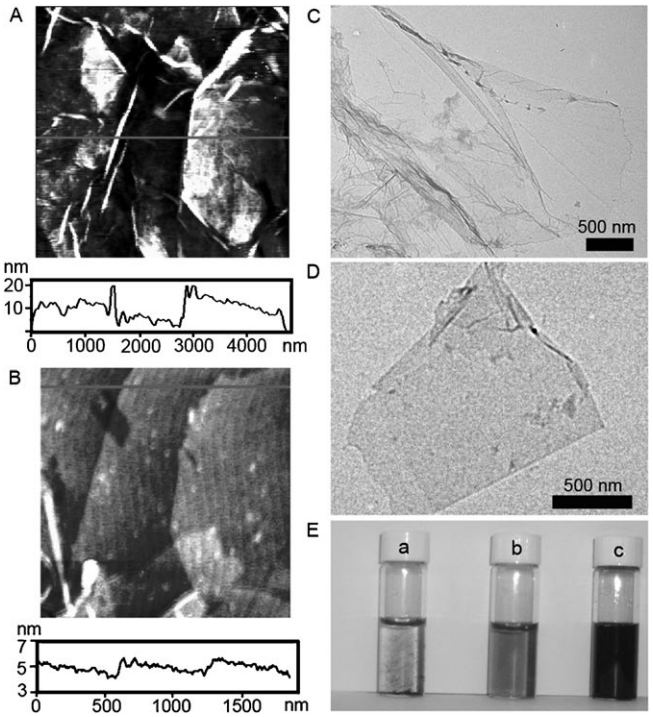

Figure 1. AFM images of A) RGO and B) FeTMAPP/RGO; TEM images of C) RGO and D) FeTMAPP/RGO; and E) photographs of a) RGO, b) FeTMAPP, and c) FeTMAPP/RGO (0.1 mg mL^{-1}) dispensed in water.

Raman and ultraviolet-visible absorption spectra of FeTMAPP/RGO: The Raman spectrum of RGO showed a disorder-induced D band at 1347 cm^{-1} arising from sp^3-hybridized carbon and a tangential stretch G band at 1576 cm^{-1} representing the E_{2g} zone center mode of the crystalline graphite (Figure 2A, curve a), which indicated significant

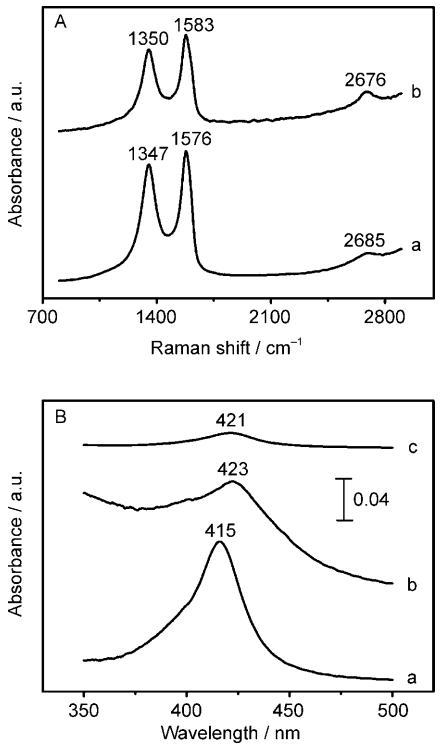

Figure 2. A) Raman spectra of a) RGO and b) FeTMAPP/RGO. B) UV/Vis absorption spectra of a) FeTMAPP, b) FeTMAPP/RGO, and c) FeTMAPP/SWNTs.

edge-plane-like defective sites existing on the surface of RGO.[48,49] The 2D band of RGO was at 2685 cm^{-1}, which is the most prominent feature in the Raman spectrum of graphene; its shape is highly sensitive and can be used to identify single-layer and few-layer graphene.[50] Compared with RGO, FeTMAPP/RGO showed the 2D band at a lower frequency (2676 cm^{-1}) with a more symmetric and sharper shape (Figure 2A, curve b). This suggested that the number of layers in FeTMAPP/RGO was less than that in RGO.[51] Therefore, FeTMAPP/RGO was more inclined to a single layer compared with RGO. In addition, compared with RGO, the D and G bands of FeTMAPP/RGO were slightly shifted to 1350 and 1583 cm^{-1} (Figure 2A, curve b), respectively, which could be associated with the noncovalent interactions of FeTMAPP with the RGO. Moreover, the ratios of the D band to the G band of FeTMAPP/RGO (1.12) and RGO (1.16) had no apparent difference, which indicated that the functionalization of RGO with FeTMAPP did not destroy the conjugations of RGO.

The UV/Vis absorption spectra of FeTMAPP, FeTMAPP/RGO and FeTMAPP/single-walled carbon nanotubes (SWNTs) are shown in Figure 2B. FeTMAPP exhibited a typical Soret band absorption at 415 nm (Figure 2B, curve a). In the presence of RGO, the Soret band of FeTMAPP/RGO is redshifted from 415 to 423 nm, which indicates the formation of a J-type aggregate nucleated on RGO through π–π noncovalent interactions (Figure 2B, curve b).[52] Meanwhile, the Soret band of FeTMAPP/SWNTs showed a decrease in absorption intensity with a redshift from 415 to 421 nm compared with FeTMAPP/RGO (Figure 2B, curve c). This could be attributed to the planar structure of RGO, which made the assembly of FeTMAPP on RGO through π–π interactions easier.

Fluorescence spectra and contact-angle photographs of FeTMAPP/RGO: Fluorescence spectra of FeTMAPP and the FeTMAPP/RGO suspension were carried out to further confirm the π–π interactions between RGO and FeTMAPP (Figure 3A). Upon excitation of FeTMAPP at 415 nm, a

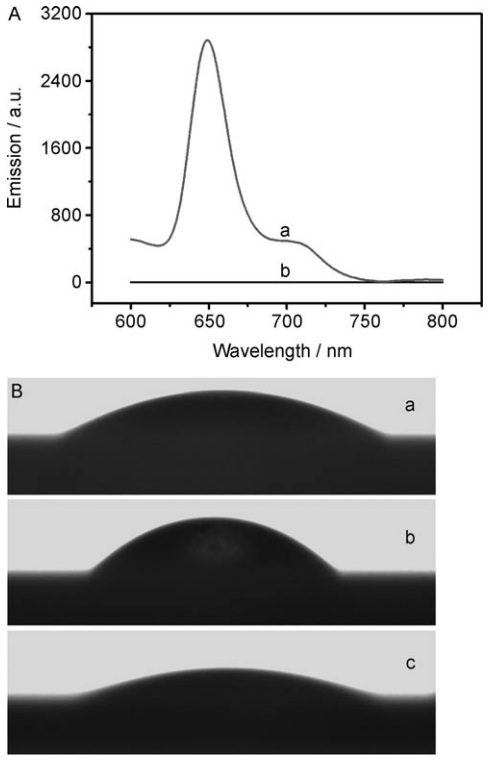

Figure 3. A) Fluorescence spectra of a) FeTMAPP (5 μM; $\lambda_{ex}=415$ nm) and b) FeTMAPP/RGO (0.1 mg mL^{-1}; $\lambda_{ex}=423$ nm) solutions. B) Contact-angle photographs of a) bare, b) RGO-, and c) FeTMAPP/RGO-modified substrates.

strong fluorescence emission peak was observed in FeTMAPP aqueous solution (Figure 3A, curve a). However, after FeTMAPP was assembled on RGO, the fluorescence emission excited at 423 nm was thoroughly quenched, and the FeTMAPP/RGO nanocomposite did not show any fluorescence (Figure 3A, curve b). The quenching efficiency was close to 100%, which could be attributed to photoinduced electron transfer from the photoexcited singlet FeTMAPP

to the RGO.[27,31] Therefore, the absorption and fluorescence spectra confirmed the good electronic communication between FeTMAPP and flattened RGO.

The biocompatibility of the novel functional material was further characterized with the contact-angle measurement. The contact angles of bare glass slide, RGO, and FeTMAPP/RGO films were measured to be 30, 47, and 23°, respectively (Figure 3B). The smaller contact angle of FeTMAPP/RGO film relative to RGO film indicated its better hydrophilicity, which added to the hydrophilic groups introduced by water-soluble FeTMAPP. The good biocompatibility of FeTMAPP/RGO could greatly improve the bioactivity of the immobilized FeTMAPP for biosensing.

Direct electrochemistry of FeTMAPP/RGO: A cyclic voltammogram of an RGO-modified ITO electrode in N_2-saturated phosphate buffer solution (PBS) showed a couple of small redox peaks (Figure 4, curve a), which resulted from

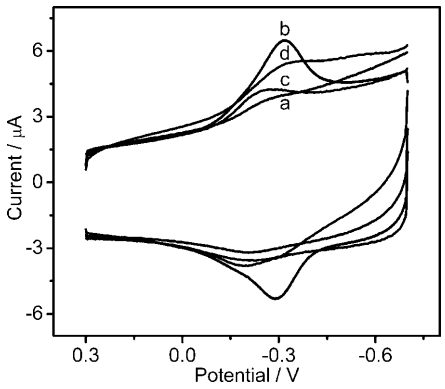

Figure 4. Cyclic voltammograms of a) RGO-, b) FeTMAPP/RGO, c) FeTMPyP/RGO-, and d) FeTMAPP/SWNTs-modified ITO electrodes in N_2-saturated PBS at 100 mV s^{-1}.

the residual surface-oxygenated species on the RGO surface during chemical reduction of GO.[48,53] The FeTMAPP/RGO-modified ITO electrode showed a couple more well-defined redox peaks at −0.291 and −0.314 V (Figure 4, curve b), which were attributed to the redox couple of Fe^{III}/Fe^{II} in immobilized FeTMAPP. The separation of peak potentials (ΔE_p) was 0.023 V, which was much smaller than that of 0.115 V for the gold nanoparticles/MWNTs–FeTMAPP-modified (MWNT = multiwalled nanotube) gold electrode,[54] thereby indicating a faster electron-transfer rate. As a control, 5,10,15,20-tetrakis(*N*-methylpyridinum-4-yl)porphyrin iron(III) pentachloride (FeTMPyP) was assembled on RGO by using the same procedure; the resulting FeTMPyP/RGO-modified ITO electrode showed a greater peak separation (Figure 4, curve c). The redox peaks with much smaller peak currents occurred at −0.198 and −0.264 V. Thus the structure of FeTMAPP was an important factor in the demonstration of fast electron transfer.

The FeTMAPP/SWNTs-modified ITO electrode also showed a pair of redox peaks with smaller peak current (Figure 4, curve d). This phenomenon was consistent with that of the UV/Vis absorption spectra, which resulted from the curved structure of SWNTs. Therefore, the presence of flattened RGO accelerated the electron transfer and increased the amount of FeTMAPP on the electrode surface. RGO as a planar sheet was a better platform for immobilizing porphyrin by means of π–π interactions, especially for picket-fence porphyrin.

The reduction and oxidation peak currents of FeTMAPP/RGO-modified electrode increased linearly as the scan rate increased from 40 to 500 mV s^{-1} (Figure 5), whereas the difference in redox peak potentials showed a slight increase, thereby indicating a surface-controlled electrode process. With an increase in the pH from 5 to 9, the oxidation potential linearly shifted to a more negative value with a slope of −53.4 mV per pH unit; this value was close to the theoretical value of −59.1 mV per pH unit at 25 °C for a one-proton and one-electron electrode process, thereby indicating that one proton participated in the redox process.

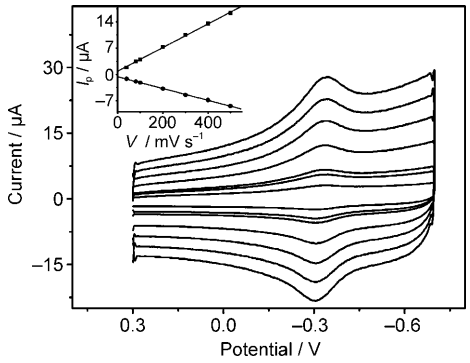

Figure 5. Cyclic voltammograms of FeTMAPP/RGO-modified ITO electrode at 40, 80, 100, 200, 300, 400, and 500 mV s^{-1} (from inner to outer) in 0.1 mol L^{-1} pH 7.0 N_2-saturated PBS. Inset: plots of oxidation and reduction peak currents versus *V*.

Electrocatalysis of FeTMAPP/RGO toward the reduction of chlorite: When chlorite (50 μmol L^{-1}) was added to PBS, no obvious catalytic peak was observed at the RGO-modified ITO electrode (Figure 6A). However, upon addition of chlorite, an enhanced catalytic reduction peak toward chlorite reduction was observed at −0.36 V with the initial potential of +0.08 V at the FeTMAPP/RGO-modified ITO electrode (Figure 6B). The electrocatalytic current was 20.28 μA, which was larger than that of the FeTMPyP/RGO-modified ITO electrode (5.49 μA; Figure 6C). This was a typical EC catalytic process,[55] in which Fe^{III}TMAPP was first reduced to iron(II) species and then back to the initial state by means of a chemical reaction with chlorite, which was finally reduced to chloride ion.[56] On the other hand, the electrocatalytic peak potential of the FeTMAPP/RGO-modified electrode (−0.36 V) for reduction of chlorite was more positive than that of the FeTMAPP/SWNTs-modified electrode (−0.55 V; Figure 6D), thus indicating a syner-

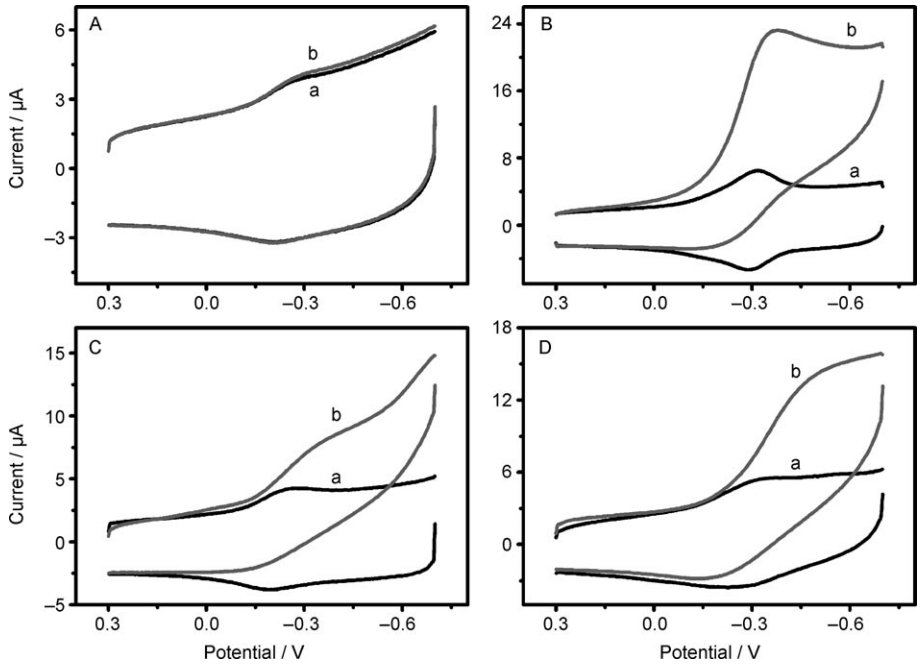

Figure 6. Cyclic voltammograms of A) RGO-, B) FeTMAPP/RGO-, C) FeTMPyP/RGO-, and D) FeTMAPP/SWNTs-modified ITO electrodes in a) 0.1 M pH 7.0 N2-saturated PBS and b) that given in (a) plus chlorite (50 μmol L^{-1}) at 100 mV s^{-1}.

gy effect of RGO and FeTMAPP in the electrocatalytic reduction of chlorite. This was an advantage for the detection of chlorite at a low applied potential, which led to a better ability to exclude the interference of other reductive species that coexisted in the samples.

With an increasing amount of deposited FeTMAPP/RGO, the reduction and oxidation peak currents for Fe^{III}/Fe^{II} increased and then tended to remain at a constant value at an amount of 5 μL (Figure 7A). At amounts higher than 10 μL, both peak currents decreased slightly due to the thicker film, which decreased the electron-transfer rate. The electrocatalytic current of chlorite reduction quickly decreased at FeTMAPP/RGO amounts higher than 10 μL (Figure 7B). This result should be attributed to the decrease in both the accessibility to catalytic sites for chlorite reduction and the electron-transfer rate. Thus, this work used a 5 μL suspension of FeTMAPP/RGO (0.1 mg mL^{-1}) to prepare the chlorite biosensor.

FeTMAPP/RGO-based biosensor for determination of chlorite: The current–time curve of the FeTMAPP/RGO-modified ITO electrode upon successive addition of chlorite at an applied potential of −0.36 V clearly illustrates the rapid response of the modified electrode to chlorite (Figure 8). The response reached a steady signal within only 4 s, and displayed a linear increase with an increase in chlorite concentration from 5.0×10^{-8} to 1.2×10^{-4} mol L^{-1} (i.e., 3.4 to 8.1×10^{3} μg L^{-1}). The detection limit was 2.4×10^{-8} mol L^{-1} (i.e., 1.6 μg L^{-1}) at a signal-to-noise ratio of 3. The linear response range was wider than those of 0.1 to 10 mg L^{-1} by capillary electrophoresis,[43] 0.02 to 2.0 μg L^{-1} by the ion chromatographic method,[44] and 50 to 150 mg L^{-1} by the potentiometric technique.[45] Thus, the proposed amperometric biosensor prepared with FeTMAPP/RGO showed promising application in the monitoring of chlorite with high sensitivity and wide concentration range.

The biosensor for chlorite showed good fabrication reproducibility, with a relative standard deviation of 4.6% estimated from the slopes of the calibration plots at five freshly prepared FeTMAPP/RGO-modified ITO electrodes. At chlorite concentrations of 0.5 and 50 μmol L^{-1}, the biosensor showed good repeatability with relative standard deviations of 5.2 and 4.7% examined for five determinations, respectively. At a chlorite concentration of

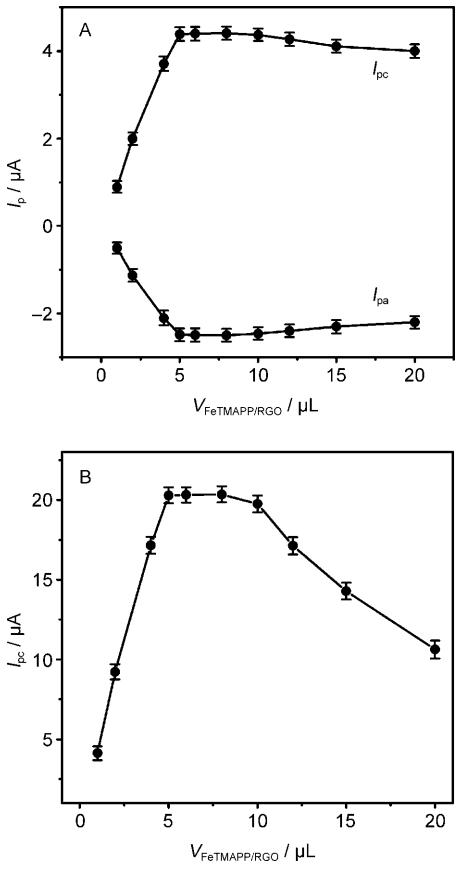

Figure 7. Effect of the amount of FeTMAPP/RGO (0.1 mg mL^{-1}) for preparation of the modified electrode on A) redox peak currents for Fe^{III}/Fe^{II} and B) electrocatalytic peak current for chlorite reduction.

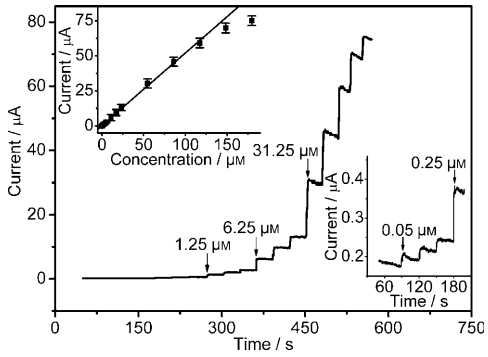

Figure 8. Successive amperometric response of FeTMAPP/RGO-modified ITO electrode to chlorite in 0.1 M pH 7.0 N_2-saturated PBS at an applied potential of −0.36 V. Upper inset: linear calibration curve; lower inset: amplified response.

50 μmol L^{-1}, the cyclic voltammograms of the biosensor for fifty consecutive scans between +0.3 and −0.7 V showed acceptable stability. The response of chlorite at the fiftieth scan remained at 97.7% of its initial response.

When the biosensor was not in use, it was stored in shade at room temperature and measured every few days. No obvious decrease in the amperometric response to chlorite was observed after one week. It was able to keep 95.8% of its initial amperometric response after four weeks. This implied that the structure of FeTMAPP/RGO was very efficient for retaining the activity of FeTMAPP and preventing it from leaking out of the biosensor.

The effects of common interfering species on the biosensing response were examined. For example, anions (F^-, Br^-, Cl^-, ClO_3^-, ClO_4^-, NO_2^-, NO_3^-, CO_3^{2-}, HCO_3^-, PO_3^{3-}, HPO_3^{2-}, $H_2PO_3^-$, SO_4^{2-}), cations (Na^+, K^+, Mg^{2+}, Zn^{2+}, NH_4^+), and saccharides (sucrose, glucose, fructose) at 1000 times the concentration of chlorite did not interfere with the amperometric response to chlorite. Ascorbic acid and lactic acid could be tolerated at less than 100 times the concentration of chlorite. Uric acid and acetic acid could be tolerated at less than 200 times the concentration of chlorite. Hypochlorite could be tolerated at less than 50 times the concentration of chlorite. Thus, the amperometric biosensor had an excellent specificity for the highly sensitive detection of chlorite without any sample pretreatment.

Conclusion

A functional nanocomposite of RGO with water-soluble picket-fence iron porphyrin was prepared by means of π–π interactions. The FeTMAPP/RGO nanocomposite had good biocompatibility and could be well dispersed in water to form a stable and homogeneous suspension due to the introduction of a positively charged FeTMAPP monolayer onto the surface of RGO. The planar side of picket-fence porphyrin reduced the distance between the porphyrin plane and flattened RGO, thus resulting in a fast electronic communication between FeTMAPP and flattened RGO. Therefore, the direct electrochemistry that corresponded to the redox couple of Fe^{III}/Fe^{II} was realized. The RGO/FeTMAPP-modified ITO electrode showed excellent electrocatalytic activity toward reduction of chlorite at low applied potential, which resulted in highly sensitive amperometric biosensing with good analytical performance for the detection of chlorite, such as rapid response, wide linear range, low detection limit, and good fabrication reproducibility. The assembly of porphyrin on RGO not only provides a facile way to design novel biofunctional nanomaterials for electrocatalysis and amperometric biosensing, but also can be extended to other optoelectronic devices.

Experimental Section

Materials and reagents: Graphene oxide was synthesized from graphite by a modified Hummers method.[57] Reduced graphene oxide (RGO) was prepared by the chemical reduction of graphene oxide with hydrazine hydrate.[20] FeTMAPP was prepared according to the work of Collman et al.[58] MS (ESI): *m/z* found for $C_{64}H_{72}Cl_4FeN_{12}O_4$ $[M-Cl]^+$: 1268; HRMS (ESI): *m/z* calcd for $C_{64}H_{72}Cl_4FeN_{12}O_4$ $[M-Cl]^+$: 1268.3903; found: 1268.3926. SWNTs (>90%, diameter <2 nm) were purchased from Shenzhen Nanotech Co. (China). Sodium chlorite (80%) was purchased from Alfa Aesar China Ltd. (China). FeTMPyP was a gift from Professor Osamu Ikeda at Kanazawa University (Japan). All other chemicals were of analytical grade. Aqueous solutions were prepared with twice-distilled water. PBS (0.1 mol L^{-1}) was always employed as the supporting electrolyte deaerated with high-purity nitrogen. The pH value of PBS was 7.0 except where indicated.

Apparatus: The TEM images was obtained using a JEM-2100 TEM instrument (JEOL, Japan). Resonance Raman spectra were recorded using a Renishaw-inVia Raman microscope (Renishaw, United Kingdom). The morphologies of the modified surfaces were studied using atomic force microscopy (Agilent 5500 model, USA) in tapping mode. Fluorescence spectra were recorded at room temperature using a F900 fluorescence spectrometer (Edinburgh Instruments Ltd., United Kingdom). UV/Vis absorption spectra were recorded using a Lambda 35 UV/Vis spectrometer (Perkin–Elmer instruments, USA). The static water contact angles were measured with a contact-angle meter (Rame-Hart-100, USA) by using droplets of deionized water at 25°C. Cyclic voltammetric and amperometric experiments were performed using a CHI 660D electrochemical workstation (CH Instruments Inc., USA). All experiments were carried out at room temperature using a conventional three-electrode system with an indium–tin oxide (ITO) electrode as a working electrode, a platinum wire as an auxiliary electrode, and a saturated calomel electrode as a reference electrode.

Preparation of FeTMAPP/RGO and the modified ITO electrodes: RGO (6 mg) and twice-distilled water (5 mL) were successively added to the FeTMAPP solution (1 mL, 3 mmol L^{-1}). The resulting suspension was ultrasonically dispersed for 1 h, and then centrifuged at 10000 rpm for 20 min to remove free FeTMAPP. After washing 5 times with twice-distilled water, the sediment was dried at 70°C to obtain the FeTMAPP/RGO nanocomposite. The as-prepared nanocomposite was ultrasonically dispersed in twice-distilled water to obtain a FeTMAPP/RGO suspension (0.1 mg mL^{-1}).

After the ITO electrode had been cleaned with NaOH (0.1 mol L^{-1}) and H_2O_2, washed with acetone and twice-distilled water, and dried at room temperature, a suspension of FeTMAPP/RGO (5 μL, 0.1 mg mL^{-1}) was coated on the ITO electrode and dried at room temperature to obtain the FeTMAPP/RGO-modified electrode. Similarly, RGO-, FeTMPyP/RGO-, and FeTMAPP/SWNTs-modified ITO electrodes were prepared.

Acknowledgements

This research was financially supported by National Basic Research Program of China (2010CB732400), the National Science Funds for Creative Research Groups (20821063), the Major Research Plan Key and General Program (90713015, 20835006, 20875044, 20705012) from the National Natural Science Foundation of China, and the PhD Fund for Young Teachers (20070284052).

[1] A. K. Geim, *Science* **2009**, *324*, 1530.
[2] A. K. Geim, K. S. Novoselov, *Nat. Mater.* **2007**, *6*, 183.
[3] C. G. Lee, X. D. Wei, J. W. Kysar, J. Hone, *Science* **2008**, *321*, 385.
[4] N. Tombros, C. Jozsa, M. Popinciuc, H. T. Jonkman, B. J. V. Wees, *Nature* **2007**, *448*, 571.
[5] C. N. R. Rao, A. K. Sood, K. S. Subrahmanyam, A. Govindaraj, *Angew. Chem.* **2009**, *121*, 7890; *Angew. Chem. Int. Ed.* **2009**, *48*, 7752.
[6] D. A. Dikin, S. Stankovich, E. J. Zimney, R. D. Piner, G. H. B. Dommett, G. Evmenenko, S. T. Nguyen, R. S. Ruoff, *Nature* **2007**, *448*, 457.
[7] V. V. Cheianov, V. Fal'ko, B. L. Altshuler, *Science* **2007**, *315*, 1252.
[8] C. Gómez-Navarro, M. Burghard, K. Kern, *Nano Lett.* **2008**, *8*, 2045.
[9] Q. L. Bao, H. Zhang, Y. Wang, Z. H. Ni, Y. L. Yan, Z. X. Shen, K. P. Loh, D. Y. Tang, *Adv. Funct. Mater.* **2009**, *19*, 3077.
[10] F. Wang, Y. B. Zhang, C. S. Tian, C. Girit, A. Zettl, M. Crommie, Y. R. Shen, *Science* **2008**, *320*, 206.
[11] L. H. Tang, Y. Wang, Y. M. Li, H. B. Feng, J. Lu, J. H. Li, *Adv. Funct. Mater.* **2009**, *19*, 2782.
[12] R. Salvio, S. Krabbenborg, W. J. M. Naber, A. H. Velders, D. N. Reinhoudt, W. G. van der Wiel, *Chem. Eur. J.* **2009**, *15*, 8235.
[13] S. Watcharotone, D. A. Dikin, S. Stankovich, R. Piner, I. Jung, G. H. B. Dommett, G. Evmenenko, S. E. Wu, S. F. Chen, C. P. Liu, S. T. Nguyen, R. S. Ruoff, *Nano Lett.* **2007**, *7*, 1888.
[14] Q. Liu, Z. F. Liu, X. Y. Zhang, L. Y. Yang, N. Zhang, G. Pan, S. G. Yin, Y. S. Chen, J. Wei, *Adv. Funct. Mater.* **2009**, *19*, 894.
[15] X. Wang, L. J. Zhi, K. Müllen, *Nano Lett.* **2008**, *8*, 323.
[16] Z. F. Liu, Q. Liu, Y. Huang, Y. F. Ma, S. G. Yin, X. Y. Zhang, W. Sun, Y. S. Chen, *Adv. Mater.* **2008**, *20*, 3924.
[17] C. H. Lu, H. H. Yang, C. L. Zhu, X. Chen, G. N. Chen, *Angew. Chem.* **2009**, *121*, 4879; *Angew. Chem. Int. Ed.* **2009**, *48*, 4785.
[18] S. J. He, B. Song, D. Li, C. F. Zhu, W. P. Qi, Y. Q. Wen, L. H. Wang, S. P. Song, H. P. Fang, C. H. Fan, *Adv. Funct. Mater.* **2010**, *20*, 453.
[19] N. Mohanty, V. Berry, *Nano Lett.* **2008**, *8*, 4469.
[20] D. Li, M. B. Müller, S. Gilje, R. B. Kaner, G. G. Wallace, *Nat. Nanotechnol.* **2008**, *3*, 101.
[21] G. Eda, G. Fanchini, M. Chhowalla, *Nat. Nanotechnol.* **2008**, *3*, 270.
[22] S. Gilje, S. Han, M. Wang, K. L. Wang, R. B. Kaner, *Nano Lett.* **2007**, *7*, 3394.
[23] J. T. Robinson, F. K. Perkins, E. S. Snow, Z. Q. Wei, P. E. Sheehan, *Nano Lett.* **2008**, *8*, 3137.
[24] E. Bekyarova, M. E. Itkis, P. Ramesh, C. Berger, M. Sprinkle, W. A. de Heer, R. C. Haddon, *J. Am. Chem. Soc.* **2009**, *131*, 1336.
[25] Y. C. Si, E. T. Samulski, *Nano Lett.* **2008**, *8*, 1679.
[26] Z. Liu, J. T. Robinson, X. M. Sun, H. J. Dai, *J. Am. Chem. Soc.* **2008**, *130*, 10876.
[27] Y. F. Xu, Z. B. Liu, X. L. Zhang, Y. Wang, J. G. Tian, Y. Huang, Y. F. Ma, X. Y. Zhang, Y. S. Chen, *Adv. Mater.* **2009**, *21*, 1275.
[28] Z. B. Liu, Y. F. Xu, X. Y. Zhang, X. L. Zhang, Y. S. Chen, J. G. Tian, *J. Phys. Chem. B* **2009**, *113*, 9681.
[29] X. L. Li, X. R. Wang, L. Zhang, S. W. Lee, H. J. Dai, *Science* **2008**, *319*, 1229.
[30] Y. X. Xu, H. Bai, G. W. Lu, C. Li, G. Q. Shi, *J. Am. Chem. Soc.* **2008**, *130*, 5856.
[31] Y. X. Xu, L. Zhao, H. Bai, W. J. Hong, C. Li, G. Q. Shi, *J. Am. Chem. Soc.* **2009**, *131*, 13490.
[32] R. Hao, W. Qian, L. H. Zhang, Y. L. Hou, *Chem. Commun.* **2008**, 6576.
[33] A. Ghosh, K. V. Rao, S. J. George, C. N. R. Rao, *Chem. Eur. J.* **2010**, *16*, 2700.
[34] J. P. Collman, Y. L. Yan, J. P. Lei, P. H. Dinolfo, *Inorg. Chem.* **2006**, *45*, 7581.
[35] J. P. Collman, N. K. Devaraj, R. A. Decréau, Y. Yang, Y. L. Yan, W. Ebina, T. A. Eberspacher, C. E. D. Chidsey, *Science* **2007**, *315*, 1565.
[36] S. Yoshimoto, K. Sato, S. Sugawara, Y. Chen, O. Ito, T. Sawaguchi, O. Niwa, K. Itaya, *Langmuir* **2007**, *23*, 809.
[37] C. Rovira, M. Parrinello, *Chem. Eur. J.* **1999**, *5*, 250.
[38] W. W. Tu, J. P. Lei, L. Ding, H. X. Ju, *Chem. Commun.* **2009**, 4227.
[39] W. W. Tu, J. P. Lei, H. X. Ju, *Chem. Eur. J.* **2009**, *15*, 779.
[40] B. Steiger, F. C. Anson, *Inorg. Chem.* **2000**, *39*, 4579.
[41] J. P. Collman, R. Boultaov, C. J. Sunderland, I. M. Shiryaeva, K. E. Berg, *J. Am. Chem. Soc.* **2002**, *124*, 10670.
[42] *Guidelines for Drinking Water Quality*, 3rd ed., World Health Organization, Geneva, **1996**, p. 989.
[43] S. R. Wallenborg, S. M. Dorholt, A. Faibushevich, C. E. Lunte, *Electroanalysis* **1999**, *11*, 362.
[44] B. H. Zhu, Z. X. Zhong, J. Yao, *J. Chromatogr. A* **2006**, *1118*, 106.
[45] L. C. Adam, G. Gordon, *Anal. Chem.* **1995**, *67*, 535.
[46] H. H. Wang, D. X. Han, N. Li, K. E. Li, *J. Inclusion Phenom. Macrocyclic Chem.* **2005**, *52*, 247.
[47] C. S. Shan, H. F. Yang, J. F. Song, D. X. Han, A. Ivaska, L. Niu, *Anal. Chem.* **2009**, *81*, 2378.
[48] M. Zhou, Y. M. Zhai, S. J. Dong, *Anal. Chem.* **2009**, *81*, 5603.
[49] D. C. Wei, Y. Q. Liu, H. L. Zhang, L. P. Huang, B. Wu, J. Y. Chen, G. Yu, *J. Am. Chem. Soc.* **2009**, *131*, 11147.
[50] D. Graf, F. Molitor, K. Ensslin, C. Stampfer, A. Jungen, C. Hierold, L. Wirtz, *Nano Lett.* **2007**, *7*, 238.
[51] Z. H. Ni, H. M. Wang, J. Kasim, H. M. Fan, T. Yu, Y. H. Wu, Y. P. Feng, Z. X. Shen, *Nano Lett.* **2007**, *7*, 2758.
[52] J. Y. Chen, C. P. Collier, *J. Phys. Chem. B* **2005**, *109*, 7605.
[53] M. Zhou, Y. L. Wang, Y. M. Zhai, J. F. Zhai, W. Ren, F. Wang, S. J. Dong, *Chem. Eur. J.* **2009**, *15*, 6116.
[54] Y. Liu, Y. L. Yan, J. P. Lei, F. Wu, H. X. Ju, *Electrochem. Commun.* **2007**, *9*, 2564.
[55] A. J. Bard, L. R. Faulkner, *Electrochemical Methods*, Wiley, New York, **2001**, pp. 473–475.
[56] I. Fabian, G. Gordon, *Inorg. Chem.* **1992**, *31*, 2144.
[57] N. I. Kovtyukhova, P. J. Ollivier, B. R. Martin, T. E. Mallouk, S. A. Chizhik, E. V. Buzaneva, A. D. Gorchinskiy, *Chem. Mater.* **1999**, *11*, 771.
[58] J. P. Collman, R. R. Gagne, T. R. Halbert, J.-C. Marchon, C. A. Reed, *J. Am. Chem. Soc.* **1973**, *95*, 7868.

Received: March 10, 2010
Published online: July 21, 2010

